CSMA 2024
16ème Colloque National en Calcul des Structures
13-17 mai 2024, Presqu'île de Giens (Var)

Fixtureless geometric inspection of slightly deformed non-rigid structures leveraging assembly load techniques

S. Sattarpanah Karganroudi[1], V. François [1], J.-C. Cuillière[1]
[1] *ERICCA, Université du Québec à Trois-Rivières, Trois-Rivières, Québec, Canada, {sattarpa,francois,jean-christophe.cuilliere}@uqtr.ca*

Summary — 3D geometric inspection ensures structural quality. Non-rigid structures tend to deform under their weight, presenting challenges in geometric inspection in a free-state. While specialized fixtures with permissible loads can maintain the functional shape of non-rigid structures, setting fixtures up is complex and time-consuming. Here, a fixtureless inspection method is introduced that leverages 3D data acquisition tools and utilizes finite element and optimization techniques to estimate restraining loads and assess the feasibility of slightly deformed non-rigid structures.
Keywords — Computer-aided inspection (CAI), fixtureless inspection, non-rigid optimization, FEA.

1. Introduction

In the field of structural analysis and finite element methods (FEM), Geometric Dimensioning and Tolerancing (GD&T) [1] assumes a crucial role in upholding the quality and performance of manufactured components. The initiation of geometric dimensioning involves the meticulous assignment of appropriate tolerances, taking into account the unique properties, intended functionality, and intricacies of the manufacturing process for each component. Despite the strides made in manufacturing processes, quality control remains labor-intensive, especially when inspecting non-rigid structures like thin-walled sheet metal components [2]. The non-rigid structural variations can be attributed to manufacturing imperfections like the spring-back effect and residual stress, challenges related to handling and transportation, including plastic deformation, and intricacies arising from assembly processes, such as deformation due to localized overheating during welding [3]. This challenge assumes particular prominence within industries like aerospace and automotive, where precision is paramount.

Within the context of 3D geometric metrology standards like ASME Y14.5 and ISO-GPS, the notion of free-state inspection necessitates that the component be placed on an inspection table without any physical constraints. However, evaluating GD&T for non-rigid components introduces inherent complexities due to the deformations that these parts undergo when subjected to a free-state inspection. Specialized physical inspection fixtures equipped with constraints and permissible loads are deemed indispensable to overcome these challenges and preserve the component's intended functional shape. This approach facilitates the retrieval of the functional component shape, even in cases where free-state deformations surpass the specified tolerances [4]. In practical terms, this geometric inspection often involves the strategic application of limited forces or weights, exemplified by sandbags, as illustrated in Figure 1. Notably, engineering design drawings frequently include notations that specify permissible loads and the required fixtures, granting authorization for their utilization during inspection.

The setup of these costly fixtures demands the expertise of skilled technicians and entails a time-consuming process of finely tuning numerous degrees of freedom to secure the part in place. Nonetheless, ongoing research endeavors are pioneering the development of fixtureless inspection methods, with the primary objective of diminishing the reliance on intricate and expensive fixtures. Advancements in non-contact 3D data acquisition tools, such as laser and optical scanners, in

conjunction with computational techniques, have propelled the field of computer-aided inspection (CAI) [5]. These CAI methods leverage scanners to capture a 3D point cloud representing the surface of a part in its free-state. A triangular mesh is generated from this point cloud to depict the part's shape. Inspection involves a virtual comparison of this scan mesh with the nominal CAD model to evaluate geometric deviations within the specified tolerances.

Figure 1 – Aerospace panel achieves functional shape under permissible loads (black sandbags) [4].

Fixtureless methods consider permissible displacements stemming from the compliance behavior of parts during assembly. The fixtureless inspection process commences with a rigid registration step, where a transformation matrix aligns the CAD and scan models. Subsequently, these methods distinguish between flexible deformation in a free-state and deviations linked to defects, virtually compensating for flexible deformation to estimate defects concerning the CAD model. However, it's worth noting that these fixtureless methods often do not account for assembly loads, which are practically applied to position geometrically deviated non-rigid parts into an assembly-ready state. This flexibility allows parts with defects exceeding geometrical tolerances to be accepted within the tolerance ranges required for assembly, demonstrating the adaptability and efficiency of these methods.

2. Virtual Mounting Assembly-State Inspection method (VMASI)

This research introduces a fixtureless inspection method, Virtual Mounting Assembly-State Inspection (VMASI) [4], inspired by techniques using weights. As depicted in Figure 2, VMASI aims to determine the feasibility of assembling slightly deviated (linear deformation) parts within assembly tolerances. VMASI creates a virtual fixture based on the GD&T specifications of CAD model to recover the functional shape of a slightly deviated part in assembly-state. It estimates the required restraining loads limited to permissible assembly loads, oriented as pressures in the gravity direction to mimic the weight of sandbags. The method partitions the scan mesh of the deviated part into zones for introducing estimated pressures. The pressures are estimated by minimizing distance and orientation differences between assembly mounting holes on the scan mesh and nominal mounting holes on the CAD model. We have termed this process the Restraining Pressures Optimization (RPO) [4] approach.

2.1. Pre-registration and preparation phase

First, a triangulated mesh is generated from the 3D scanned point cloud in STL format. This mesh is then processed to reduce scanning noise and size by applying smoothing and simplification techniques. To evaluate the impact of different defect types, shapes, and amplitudes, synthetic defects are introduced into the CAD model, allowing precise control over their characteristics.

The pre-registration phase involves a rigid registration process using the iterative closest point (ICP)

algorithm [6], aligning the datums on the scan mesh with those on the CAD mesh. Subsequently, the scan mesh is partitioned into $N_{\mathcal{P}}$ zones, represented by lists of connected triangles in each partition. This partitioning can be automated using Voronoi tessellation [7] or performed manually by separating and partitioning connected triangles for each zone.

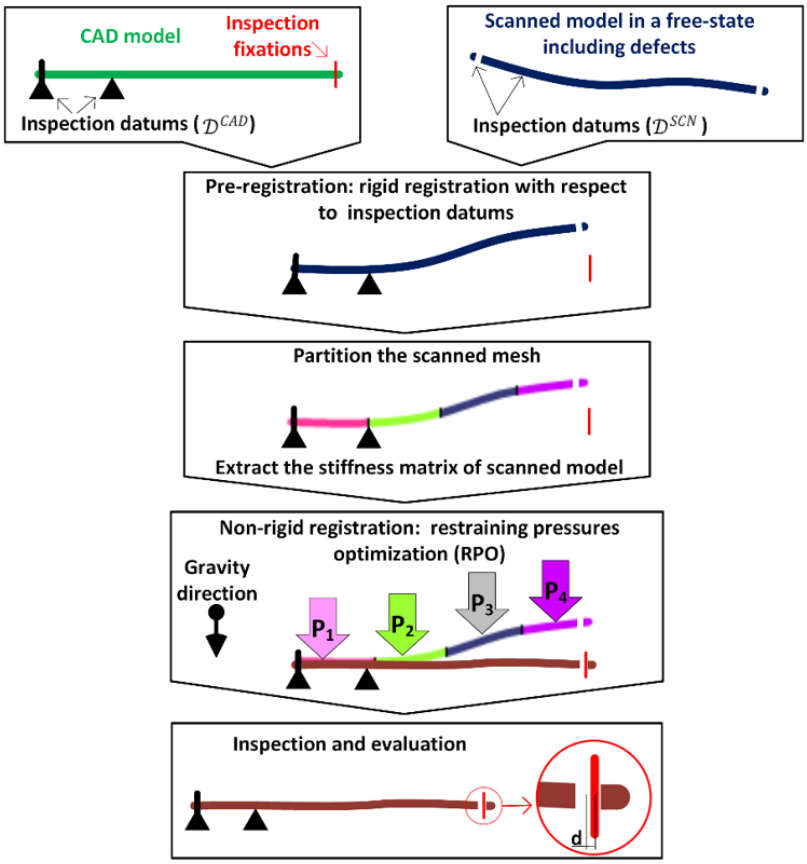

Figure 2 – Flowchart and 2D schematic of the proposed virtual mounting assembly-state inspection method [4].

2.2. Non-rigid registration

Given their compliant characteristics, non-rigid components often deviate from the nominal CAD geometry in a free-state, which can significantly affect their final assembly fit. To address this, the aligned and partitioned scan mesh undergoes virtual deformation to match the CAD mesh, positioning it in the assembly-state. This deformation is accomplished by applying permissible forces on the scan mesh through finite element analysis (FEA), using a linear FE-based transformation [8] represented as:

$$\{f\}=[K]\{u\} \quad (1)$$

where {f} represents the force vector, [K] stands for the global stiffness matrix, and {u} is the displacement vector. In inspecting non-rigid components, this study focuses on using flat, thin sheet metals, where the plates are thin relative to their lateral dimensions. To analyze such structures, plate FEA is employed based on Kirchhoff-Love (K-L) Plate Theory, which is suitable for thin plates subjected to moderate loads. We utilize the Discrete-Kirchhoff triangular (DKT) element modeling approach. This method operates under the assumption that plates experience small displacements and strains, and it incorporates the principle that zero transverse shear strain is satisfied at specific discrete points within the element. This inclusion of shear deformation effects makes Kirchhoff plate elements suitable for application in thin and thick plates [9, 10]. DKT elements of Code_Aster™ software [11] are employed in this study, having only five degrees of freedom (DOF) at the corner nodes of the

midplane, represented by in-plane u, v and transverse w displacements as well as rotational displacements θ_x, θ_y around the x and y directions, as illustrated in Figure 3.

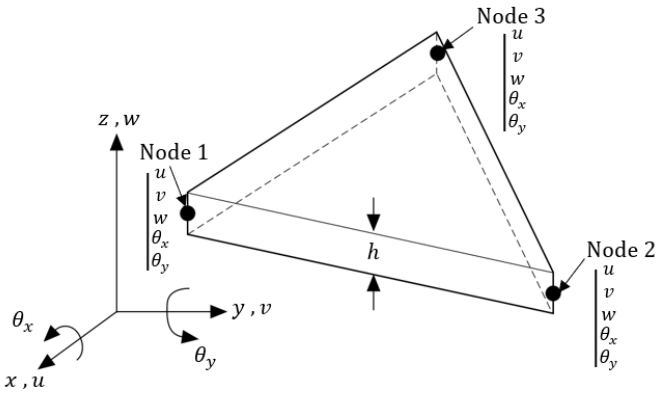

Figure 3 – A 15 DOF triangular DKT plate element [11].

Assuming that perpendicular sections to the midplane remain straight and that the displacement fields vary linearly throughout the thickness of the plate, the displacements of a point (u_x, u_y, u_z with respect to x, y, z) adhere to the Hencky-Mindlin kinematics [11]:

$$\begin{pmatrix} u_x(x,y,z) \\ u_y(x,y,z) \\ u_z(x,y,z) \end{pmatrix} = \begin{pmatrix} u(x,y) \\ v(x,y) \\ w(x,y) \end{pmatrix} + z \begin{pmatrix} \theta_y(x,y) \\ -\theta_x(x,y) \\ 0 \end{pmatrix} \tag{2}$$

Here, u, v, and w represent the displacements of the midplane, and θ_x and θ_y denote the rotations of this surface with respect to the x and y axes, respectively. The behavior of the plate in 3D is based on the assumption of plane stress, where the transverse stress σ_{zz} is considered negligible and, therefore, assumed to be zero in comparison to the other components of the stress tensor. By applying the principle of virtual work ($\delta W_{ext} = \delta W_{int}$), specifically in matrix form in elasticity ($\delta \boldsymbol{U}^T \boldsymbol{K} \boldsymbol{U} = \boldsymbol{F} \delta \boldsymbol{U}$), we obtain the stiffness matrix K. The global stiffness matrix is derived from assembling all local stiffness matrices in the global reference frame. It's important to emphasize that the global stiffness matrix is computed using Code_Aster™ software.

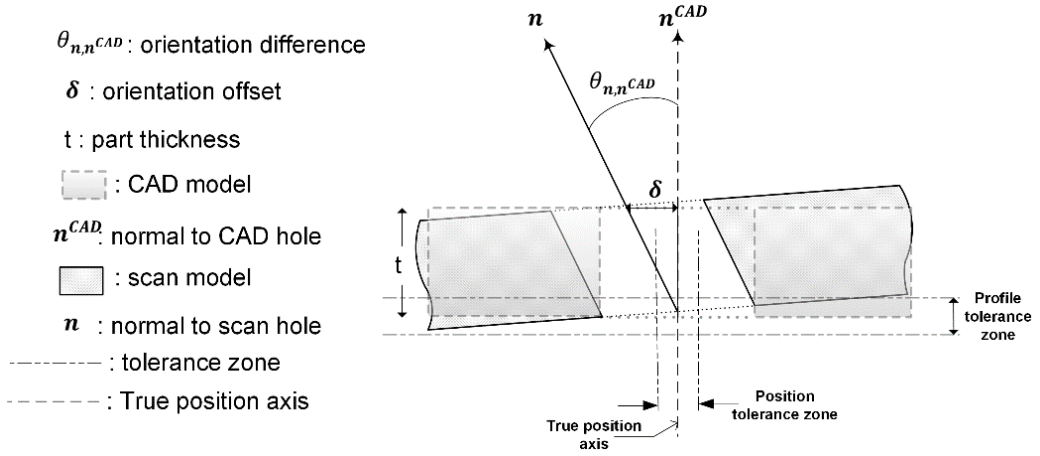

Figure 4 – Discrepancy in alignment: assembly mounting hole on predicted scan model vs. CAD model [4].

To adapt the virtual inspection method for our specific application, we simulate the practical inspection technique's weights (sandbags) as pressures applied in the direction of gravity onto the scan mesh. Consequently, we adjust the force vector in the FE calculation to account for these applied pressures on each zone of the partitioned scan mesh. This adjustment entails the calculation of pressure extrapolation to nodal forces for each triangle within the scan mesh. After establishing the FE-based transformation, we implement a non-rigid registration process called the Restraining Pressures Optimization (RPO) approach to minimize the distance and orientation differences between the mounting holes on the scan and CAD mesh. As illustrated in Figure 4, we calculate each mounting hole's center and normal vector using the nodes situated along the hole's perimeter.

To minimize distance and orientation differences, we formulate an optimization problem that aims to minimize both the Euclidean distances and the orientation disparities between the holes on the scan and CAD mesh. We calculate the center of holes on the scan mesh ($\boldsymbol{C}_i$) and CAD model ($\boldsymbol{C}_i^{CAD}$), which are centers of unit mass associated with nodes around the edge of a mounting hole in both the scan and CAD meshes. Subsequently, we compute the arithmetic average of the differences (Δ) between these centers of mass associated with the mounting holes on both the scan and CAD meshes.

$$\Delta = \frac{1}{N_{\mathcal{L}}} \sum_{i=1}^{N_{\mathcal{L}}} \left\| \boldsymbol{C}_i - \boldsymbol{C}_i^{CAD} \right\| \tag{3}$$

To compare the orientation of mounting holes on the scan mesh in comparison to those on the CAD mesh, we measure the angle between their respective normal, denoted as $\theta_{\boldsymbol{n},\boldsymbol{n}^{\boldsymbol{CAD}}}$. We calculate a root mean square deviation (O), as outlined in Equation (4), for $N_{\mathcal{L}}$ number of mounting holes.

$$O = \sqrt{\frac{1}{N_{\mathcal{L}}} \sum_{i=1}^{N_{\mathcal{L}}} (\theta_{\boldsymbol{n},\boldsymbol{n}^{\boldsymbol{CAD}}(\boldsymbol{i})})^2} \tag{4}$$

To formulate an appropriate objective function that takes into account both distance and orientation values, we introduce a weighting factor (w) to ensure a balanced consideration of these two aspects. Consequently, we derive the objective function (OF) defined in Equation (5).

$$OF(\mathcal{P}) = \Delta + (w \times O) \tag{5}$$

Here, w can be determined based on the relative proportions of the initial values for distance and orientation, as outlined in Equation (6).

$$w \approx \frac{\Delta_{initial}}{O_{initial}} \tag{6}$$

Subsequently, distance and orientation differences between the scan and CAD meshes are minimized by estimating pressures ($\mathcal{P}$) applied on $N_{\mathcal{P}}$ partitioned zones of scan mesh in the gravity direction.

$$\arg\min_{\mathcal{P}} \quad OF(\mathcal{P}) \tag{7}$$

$$subject\ to\ P_i \leq P_i^{Max}, i = 1, \dots, N_{\mathcal{P}}$$

In Equation (6), the vector $\boldsymbol{\mathcal{P}} = \langle P_1, \dots, P_{N_{\mathcal{P}}} \rangle$, where $P_i \in \mathbb{R}^+$, represents the magnitude of the gravitational pressures applied to each partitioned zone on the scan mesh. This optimization problem is tackled using a constrained nonlinear gradient-based optimization method [12]. This method relies on derivatives (gradients) of the objective function and constraints to guide the search for the optimum solution, helping determine both the direction and step size of the search. Importantly, during each optimization iteration, Equation 1, which utilizes the stiffness matrix extracted from Code_Aster™ software, is employed in each optimization iteration. As a result, the optimization process seeks to deform the scan mesh under distributed pressures (nodal forces) to minimize the distance and orientation differences between mounting holes on the scan and CAD meshes.

3. Study Case Results

In this section, a representative aerospace aluminum panel, 2.5 mm thick and approximately 1730 × 1425 mm in size (0.59 m^2 area), was inspected. The panel was initially mounted using datum targets (datum A), with further adjustments made to datum B using an adjusting pin. The part was stabilized by inserting another adjusting pin into a slotted tooling hole (datum C), located diagonally opposite datum B. The use of restraining loads like sandbags on different panel zones allowed the deviated manufactured panel to be placed in its assembly position. Conventional inspection methods employ numerous fixtures to obtain the part's functional shape, while as presented in Figure 5, our VMASI method virtually mounts deviated manufactured parts using only nine fixtures for simulating datum targets (datum A).

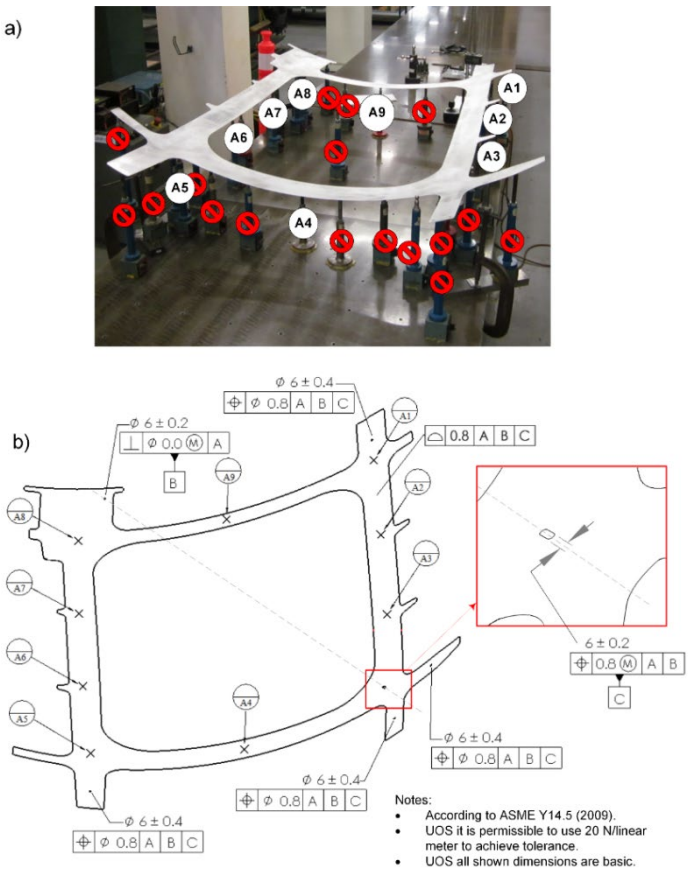

Figure 5 – a) Non-rigid panel mounted on inspection fixtures; b) GD&T specification [4].

Displacement constraints on the edges of datum B's tooling hole ensured model stability for VMASI. The RPO approach calculated the position and value of required pressures, representing weights, by minimizing distance and orientation differences of mounting holes. Inspection was conducted on these mounting holes (FIXTURE 1, 2, 3, and 4) to ensure they respect the assembly-state tolerance of ±0.4 mm (Ø0.8 mm as depicted in Figure 5-b). The maximum permissible restraining force is 20 lbf/ft2 (approximately 960 Pa), while the maximum tolerable orientation difference for mounting holes is 9 degrees, based on a constant part thickness of 2.5 mm.

In this case, the scan mesh exhibits significant deformation, with a maximum displacement of 21 mm (Figure 6-a). After partitioning the scan model, the required assembly loads are estimated using the RPO approach and detailed in Table 1. By applying these estimated pressures to the partitioned zones through a finite element-based transformation, we predict the functional shape of the scan model in its assembly-state. The assessment of mounting holes on this predicted shape concerning the nominal features in the CAD model is then conducted. The inspection results, as shown in Table 2, reveal that the profile offsets

for Feature 2 and 3 mounting holes exceed the tolerance range of ±0.4 mm. This indicates that the deviated scan model cannot be assembled satisfactorily.

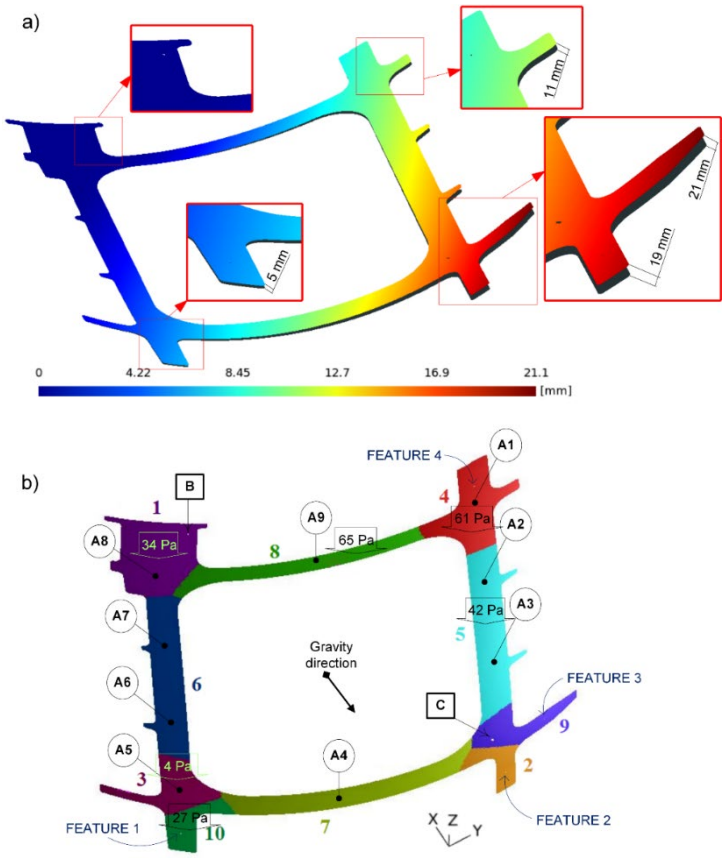

Figure 6 – a) Displacement distribution [mm] of deviated scan mesh simulating an intermediate plastic defect; b) the partitioned scan model and predicted assembly pressure [4].

Table 1 – Validation of assembly pressure and force in the case study.

Zones	Area [mm^2]	Permissible pressures [Pa]	Pressure [Pa]	Force [N]
1	79536	960	34	2.71
2	27417	960	0	0.00
3	47631	960	4	0.19
4	64296	960	61	3.91
5	87768	960	42	3.69
6	79928	960	0	0.00
7	80779	960	0	0.03
8	52096	960	65	3.38
9	42550	960	0	0.00
10	30069	960	27	0.81

4. Conclusion

This research introduces a novel computer-aided inspection (CAI) technique called Virtual Mounting Assembly-State Inspection (VMASI), designed for fixtureless inspection of non-rigid structures. VMASI replicates a practical aerospace industry inspection method that uses weights (sandbags) to position geometrically deviated non-rigid parts into their assembly-state while constraining specific

features. The VMASI process involves a linear finite element-based transformation within a Restraining Pressure Optimization (RPO) framework, which determines the required restraining pressures on specific zones of the part to predict its optimized shape in the assembly-state. This predicted shape is then compared to the nominal CAD model to assess the positions and orientations of mounting holes. VMASI can accept or reject non-rigid parts based on these comparisons. The method uses synthetic defects on scan meshes to validate and quantify its accuracy, allowing control over defect shape, amplitude, and location. Results from applying VMASI to non-rigid parts show that part acceptance is related to defect amplitude, with highly deviated parts often being rejected.

Future work will focus on incorporating nonlinear finite element analysis into the RPO module to enhance accuracy, especially for scan models with large displacement defects. Additionally, assessing the method's robustness and handling uncertainties in the broader range of part geometries would be valuable. While the method is numerically validated using synthetic defects in this study, future research should explore its performance with real scan data acquired from scanning physical parts in free-state conditions to evaluate its real-world accuracy and effectiveness.

Table 2 – Validation results for the case study's position, profile, and orientation.

Mounting holes	Position/Profile tolerance [mm]	Orientation tolerance [deg.]	Position offset [mm]	Profile offset [mm]	Orientation difference [deg.]
Feature 1	Ø0.8 mm (±0.4mm)	9 deg.	0.01 (accepted)	0.28 (accepted)	0.13 (accepted)
Feature 2	Ø0.8 mm (±0.4mm)	9 deg.	0.10 (accepted)	0.43 (rejected)	0.06 (accepted)
Feature 3	Ø0.8 mm (±0.4mm)	9 deg.	0.05 (accepted)	0.47 (rejected)	0.06 (accepted)
Feature 4	Ø0.8 mm (±0.4mm)	9 deg.	0.01 (accepted)	0.06 (accepted)	0.17 (accepted)

References

1. Tornincasa S, Tornincasa S (2021) Geometrical specification for non-rigid parts. Tech Draw Prod Des Mastering ISO GPS ASME GD&T 283–290
2. Aminzadeh A, Sattarpanah Karganroudi S, Meiabadi MS, et al (2022) A Survey of Process Monitoring Using Computer-Aided Inspection in Laser-Welded Blanks of Light Metals Based on the Digital Twins Concept. Quantum Beam Sci 6:19. https://doi.org/10.3390/QUBS6020019
3. Bogdan PAM, John V V (2022) Applying Engineering Techniques on Non-Traditional Real-World Problems. In: 2022 IEEE Integrated STEM Education Conference (ISEC). IEEE, pp 233–237
4. Sattarpanah Karganroudi S, Cuillière J-CC, François V, Tahan S-AA (2018) "What-if" scenarios towards virtual assembly-state mounting for non-rigid parts inspection using permissible loads. Int J Adv Manuf Technol 2018 971 97:353–373.
5. Zhu X, Hu H (2020) Computer-Aided Inspection and Quality Control System for Automotive Parts. In: Innovative Computing: IC 2020. Springer, pp 1051–1058
6. Ravishankar S, Dutt HN V, Gurumoorthy B (2010) Automated inspection of aircraft parts using a modified ICP algorithm. Int J Adv Manuf Technol 46:227–236
7. George PL, Frey P (2013) Mesh generation: application to finite elements. John Wiley & Sons
8. Batoz J-L, Dhatt G (1990) Modélisation des structures par éléments finis. Presses Université Laval
9. Brank B, Ibrahimbegović A, Bohinc U (2015) On Discrete-Kirchhoff Plate Finite Elements: Implementation and discretization error. Adv Struct Mater 45:109–131.
10. Batoz J, Bathe K, Ho L (1980) A study of three-node triangular plate bending elements. Int J Numer Methods Eng 15:1771–1812
11. Soza T (2013) Éléments de plaque: modélisations DKT–DST-DKTG et Q4G, Documentation of Code_Aster, R3. 07.03
12. Beck A (2014) Introduction to nonlinear optimization: Theory, algorithms, and applications with MATLAB. SIAM